Applied Catalysis B: Environmental 176–177 (2015) 99–106

Contents lists available at ScienceDirect

Applied Catalysis B: Environmental

journal homepage: www.elsevier.com/locate/apcatb

Non-thermal plasma synthesis of sea-urchin like α-FeOOH for the catalytic oxidation of Orange II in aqueous solution

Antoine Tiya-Djowe[a,b,*], Samuel Laminsi[b], Georges L. Noupeyi[b], Eric M. Gaigneaux[a,**]

[a] Institute of Condensed Matter and Nanosciences – IMCN, Division "MOlecules, Solids and reactiviTy – MOST", Université catholique de Louvain, Croix du Sud 2, box L7.05.17, 1348 Louvain-la-Neuve, Belgium
[b] Inorganic Chemistry Department, University of Yaoundé I, P.O. Box 812, Yaoundé, Cameroon

ARTICLE INFO

Article history:
Received 29 January 2015
Received in revised form 18 March 2015
Accepted 29 March 2015
Available online 31 March 2015

Keywords:
Gliding arc plasma
Goethite
Urchin-like nanostructures
Fenton catalyst

ABSTRACT

In this study, a template-free synthesis of iron oxyhydroxide nanostructures by gliding arc plasma at atmospheric pressure was evaluated. The results showed that exposure of a Mohr's salt solution to the plasma discharge induces a rapid oxidation–precipitation of iron(II) into a non-porous and amorphous iron(III) (hydr) oxide. After ageing in temporal post-discharge for three hours, the amorphous iron (hydr) oxide was transformed into crystalline goethite (α-FeOOH). The presence of goethite was confirmed by FTIR, Raman spectroscopy and thermogravimetric analysis. Textural analyses showed that the material is mesoporous with a BET surface area of 134 $m^2 g^{-1}$. SEM pictures revealed that the plasma-synthesized goethite particles consist of sea-urchin like hollow spheres. The catalytic activity of such goethite in the Fenton degradation of Orange II (organic dye) showed that this material can be used as heterogeneous catalyst for effective removal of organic pollutants from wastewater. This study establishes that the plasma discharge of gliding arc type can be used as a green and cheap efficient route for the synthesis of porous metal oxide nanostructures.

© 2015 Elsevier B.V. All rights reserved.

1. Introduction

During the last decade, iron (hydr) oxides have drawn significant interest for their potential applications in the field of wastewater treatment because of their demonstrated excellent adsorption and catalytic capacities, and their environmentally benign nature [1–6]. Among them, iron (hydr) oxides with three dimensional nanostructures composed of hierarchically assembled nanosized building blocks have several advantages for adsorption and catalysis, such as their high surface area and their easy separation [7–8]. However, the conventional methods used for the production of iron (hydr) oxides with hierarchical nanostructures are quite expensive because they need the use of templates such as ethylene glycol, and other chemicals including urea and tetrabutylammonium bromide [7]. Another disadvantage of these methods is that they are not environmentally friendly. To overcome the above disadvantages, Faria et al. have recently developed a new green method for the synthesis of iron oxyhydroxide with nanosized particles and high surface area [9]. Briefly, they mixed an alcoholic solution of sodium hydroxide with iron(II) solution, and then, they added hydrogen peroxide to the mixture to form a δ-FeOOH precipitate. During this process, sodium hydroxide and hydrogen peroxide were used as precipitating and oxidizing reagents, respectively. Based on this previous work, we developed a new surfactant-free method to prepare iron oxyhydroxide by using gliding arc plasma with humid air as feeding gas. Our hypothesis is that the hydroxyl radicals created by the plasma discharge can simultaneously act as oxidizing and precipitating reagents for the fabrication of iron oxyhydroxide. Indeed, Depenyou et al. highlighted the formation of lepidocrocite (γ-FeOOH) while treating a carbon steel by gliding arc plasma [10]. The plasma discharges in humid air are known to induce acidifying and oxidizing effects in an aqueous target solution. In such plasmas, a part of the thermal energy carried on by the arc is transferred to the surrounding "parent species" of the feeding gas (i.e. O_2, N_2 and H_2O) and thus favours the cleavage of H—OH and O=O bonds. This feature requires less energy than for N≡N bond breaking and allows rising gaseous moieties from their fundamental energy level to some excited state. Thus, the NO• and HO• radicals mainly

* Corresponding author.
** Corresponding author at: Institute of Condensed Matter and Nanosciences – IMCN, Division "MOlecules, Solids and reactiviTy – MOST", Université catholique de Louvain, Croix du Sud 2, box L7.05.17, 1348 Louvain-la-Neuve, Belgium.
Tel.: +32 10473665; fax: +32 10473649.
E-mail addresses: tony_tiya@yahoo.fr (A. Tiya-Djowe), eric.gaigneaux@uclouvain.be (E.M. Gaigneaux).

http://dx.doi.org/10.1016/j.apcatb.2015.03.053
0926-3373/© 2015 Elsevier B.V. All rights reserved.

formed in the arc by electron impact as shown in Eqs. (1)–(4) were identified and quantified by emission spectroscopy [11].

$$H_2O + e^- \rightarrow H^\bullet + HO^\bullet + e^- \quad (1)$$

$$H_2O + e^- \rightarrow H^+ + HO^\bullet + 2e^- \quad (2)$$

$$O_2 + e^- \rightarrow 2O^\bullet + e^- \quad (3)$$

$$N_2 + O^\bullet \rightarrow NO^\bullet + N^\bullet \quad (4)$$

The first aim of our study is to investigate whether the gliding arc plasma species (mostly $HO^\bullet$ radicals) can be used as reagents for the synthesis of hierarchical iron oxyhydroxide nanostructures. The most important merit of this process as compared with other methods consists in the fact that it only requests mild conditions and a short processing time. Moreover, this process can be considered as a green and cheap route, since the only chemical used to produce the reactive species is a water saturated air which is non-pollutant, available and renewable. The second objective of our work is to evaluate the catalytic performance of the plasma-synthesized material in the heterogeneous Fenton removal of organic pollutants from water.

The plasma-synthesized materials were characterised by X-ray powder diffraction (XRD), Fourier transform-infrared spectroscopy (FTIR), Raman spectroscopy, thermogravimetric analysis (TGA), scanning electron microscopy (SEM) and nitrogen physisorption. The catalytic performances were evaluated for the bleaching of an Orange II dye solution. Orange II is a toxic and non-biodegradable azoïc dye often present in textile and food industrial wastewater.

2. Experimental methods

2.1. Preparation of α-FeOOH nanostructures

The design of the reactor used for the preparation of iron oxyhydroxide was described in our previous works [12–14] and consists of a pair of aluminium electrodes symmetrically disposed on both sides of an atomizing nozzle (diameter = 1 mm) and connected to an AC 220 V/10kV-1A high voltage transformer which delivers a mean current of 160 mA (600 V) in operating conditions (Fig. 1). The selected feeding gas is water saturated air. Air is provided by a compressor and then saturated by water by passing through a bubbling flask maintained at 25 °C before being blown between the electrodes at a flow rate of 800 L h^{-1}. A plasma plume is generated by an electric arc formed between the electrodes when the high voltage is applied. This arc is then pushed away by the gas flow and glides along the electrodes until it collapses. A new arc is then formed and the cycle resumes. During this cycle, the length of the arc increases and its temperature decreases, so that the arc turns from a thermal plasma to a quenched plasma.

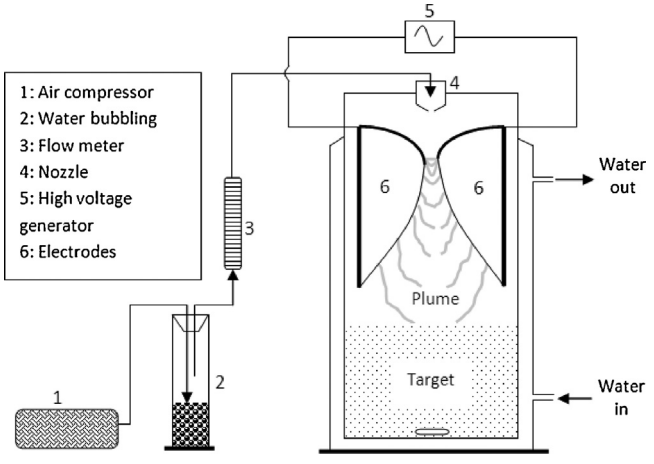

Fig. 1. Scheme of the gliding arc plasma reactor.

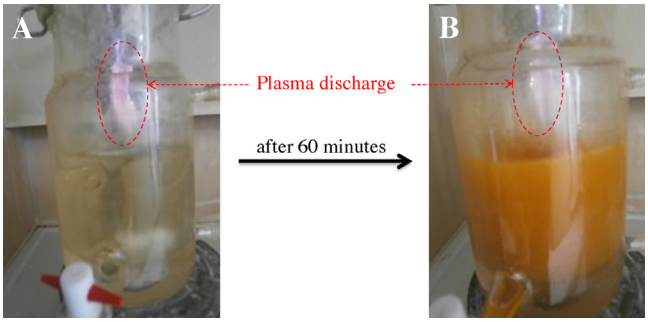

Fig. 2. The plasma reactor containing a 32.5 mM iron(II) solution before (A) and after plasma-treatment for 60 min (B); the observed yellow-brown suspension witnesses the presence of iron(III) oxide/hydroxide in the medium.

Ammonium iron(II) sulphate hexahydrate $[(NH_4)_2Fe(SO_4)_2{\cdot}6H_2O]$ (purity = 99.997%) was purchased from Sigma–Aldrich (Belgium) and was used as received. $(NH_4)_2Fe(SO_4)_2{\cdot}6H_2O$ was chosen because of its better stability to air oxidation as compared to other iron(II) salts. In a typical procedure, 13 mmol of $(NH_4)_2Fe(SO_4)_2{\cdot}6H_2O$ were dissolved in 400 mL of deionized water and disposed normally to the axis of the glass reactor (Fig. 2A) at a distance of about 2.5 cm from the electrodes tips. The reactor was cooled down by a water draught and the temperature was kept around 50 °C to limit evaporation and vapour stripping. The solution was exposed to the plasma discharge for different times t^* (i.e. 0, 15, 30, 60, and 120 min) under magnetic stirring. During this process, the pH of the medium was measured in order to follow the acidification of the target solution exposed to the plasma discharge. After the discharge was switched off, the obtained precipitate was collected by vacuum filtration using a 0.45 μm millipore filter, washed with deionized water and dried at 80 °C for 24 hours. The powder obtained after each exposure time was weighted. For the optimum exposure time predetermined, the yellow-brown precipitate obtained (Fig. 2B) was further aged in the reactor at 98 °C for 1–3 h with plasma shut off before being collected. The obtained products were, respectively, named as A1–A3. The non-aged material was named as A0.

2.2. Characterizations

X-ray diffraction (XRD) analyses were performed on a Siemens D5000 diffractometer using the Kα radiation of Cu (λ = 1.5418 Å). The 2θ range was recorded between 5° and 70° at a rate of 0.02 °s^{-1}. The ICDD–JCPDS database was used to identify the crystalline phases. The Fourier transform-infrared spectra were recorded using an Equinox IFS55 spectrometer (Brücker) equipped with a DTGS detector. The absorption spectra were obtained by the recording of 100 scans between 400 and 4000 cm^{-1} with a resolution of 4 cm^{-1}. The powders were diluted in an analytical grade KBr (Janssens Chimica 99%) by a weight factor of 100, and then pressed into self-supporting disks before analysis. SEM micrographs were taken with a LEO 983 GEMINI microscope equipped with a field emission gun. The uncoated samples were exposed to an acceleration voltage of 1 kV. Textural analyses were carried out on Micromeritics Tristar 3000 equipment using N_2 adsorption/desorption at −196 °C. Before measurement, the samples were outgassed at 90 °C overnight under vacuum. The specific surface area was calculated using the Brunauer–Emmet–Teller (BET) equation whereas the pore size distributions were derived from the desorption branches using the Barrett–Joyner–Halenda (BJH) model. Confocal Raman spectroscopy was done on DXR Raman

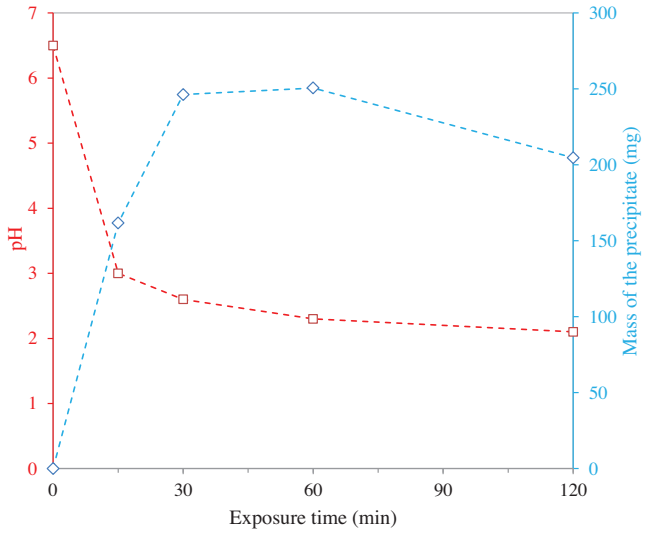

Fig. 3. Evolution of the mass of precipitate and pH of the aqueous suspension as a function of exposure time during the plasma synthesis process.

microscope (Thermo Nicolet) equipped with a diode light (780 nm). The resolution was set to 4 cm^{-1}. The number of scans was 10 and the time of accumulation was 10 s per scan. The laser power was set to 10 mW and the 50× objective was used. The thermogravimetric analysis was performed on a Mettler Toledo TGA/SDTA 851 machine. For this purpose, about 3.5 mg of the sample was heated in an air stream (110 mL min^{-1}) from 30 °C to 600 °C at a 10 °C min^{-1} rate.

2.3. Catalytic properties

The sample A3 was tested as a catalyst for heterogeneous Fenton bleaching of Orange II (OII) dye in aqueous solution. For this purpose, a 25 mg L^{-1} solution of OII was prepared and the pH was adjusted to 3 with 0.1 M solution of H_2SO_4. The as-prepared material (40 mg) was added to 250 mL Erlenmeyer flask containing 200 mL of the above OII solution. The reaction was initiated by the addition of 0.1 mL of H_2O_2 30% (Sigma–Aldrich). The temperature of the medium was kept at 30 °C using a water bath. At specific time intervals, 2 mL aliquots of the solution were withdrawn from the reaction mixture and filtrated using a 0.2 μm PTFE membrane. UV–vis absorption spectra were recorded at different intervals to monitor the bleaching process using a Beckman Coulter D800 spectrophotometer. The OII concentration evolution was observed from its characteristic absorption wavelength at 485 nm. A commercial iron oxyhydroxide (goethite, Sigma–Aldrich, S_{BET} = 35 m^2 g^{-1}) was also adopted as the reference to compare the catalytic activity under the same experimental conditions. In order to evaluate the mineralisation of OII, the Total Organic Carbon (TOC) was also measured. The instrument used for this purpose was a Shimadzu TOC-L apparatus.

3. Results and discussion

3.1. Preparation and characterization of iron oxyhydroxide

Fig. 3 shows the evolution of the solution pH as a function of the exposure time of the iron(II) solution to the plasma discharge. The initial solution pH was 6.5. When the reaction proceeds, the pH of the solution decreases drastically during the first 30 min. It then stabilizes around 2.2 after 1 h. This decrease in pH is a consequence of the acidifying properties of humid air plasma as described in previous works [15,16]. Such properties are mainly due to the transformation of NO• radicals into transient nitrous acid (ONOH) which, at pH < 6, disproportionates into nitric acid (HNO_3). Fig. 3 also reveals an increase in precipitate mass with increasing exposure time. The maximum mass obtained was 250 mg after 60 min. Further increase in exposure time did not increase the precipitate quantity, likely because of the establishment of an equilibrium between the formation of the precipitate and its dissolution due to the acidity of the medium. Hence, the acidifying properties of humid air plasma are herein considered as an unwanted phenomenon according to its negative effect on the synthesis yield. In the following of the work, 60 min was thus chosen as the optimum exposure time for the plasma synthesis of iron (hydr) oxide.

The powder X-ray diffraction patterns (XRD) of the fresh and the aged products are depicted on Fig. 4A. This figure reveals that the product obtained without ageing (i.e. A0) was poorly crystalline. However, the degree of crystallinity of the product was improved with increased ageing time. The XRD pattern of the material obtained after ageing for 3 h (i.e. A3) indicates the presence of goethite (α-FeOOH) as the main crystalline phase (JCPDS 29-0713). The XRD results are in agreement with FTIR measurements (Fig. 4B). Indeed, the FTIR spectrum of the sample A3 presents bands at 884 cm^{-1} and 792 cm^{-1} which characteristic of hydroxyl bending vibrations in goethite [17]. These bands were absent for the non-aged sample (A0) and appeared along the ageing process. At the same time, the bands intensities of the amorphous hydroxide (clearly visible in sample A0) at 1124 cm^{-1} and 986 cm^{-1} gradually decreased along the ageing process whereas that at 698 cm^{-1} was totally disappeared for the A3 sample. The strong bands at 616 cm^{-1}

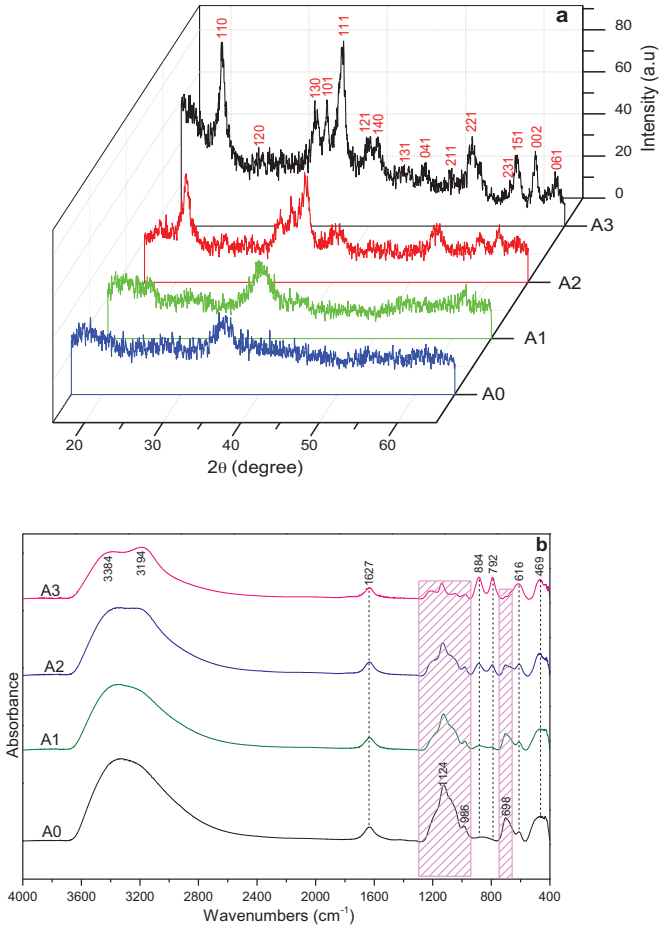

Fig. 4. XRD pattern (a) and FTIR spectrum (b) of the plasma synthesized product and its evolution with ageing time.

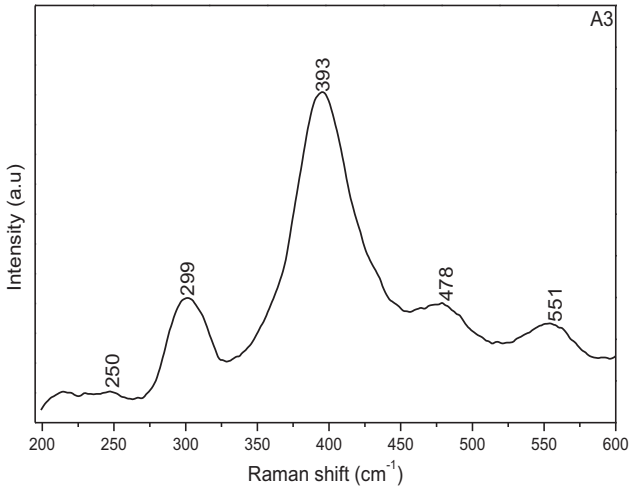

Fig. 5. Confocal Raman spectrum of the 3 h aged plasma-synthesized material (A3) showing the characteristic Raman shifts of goethite.

and 469 cm^{-1} which were also present on the spectrum of the non-aged sample correspond to Fe—O stretching and bending vibration modes, respectively. From Fig. 4B, it can also be seen that the spectrum of sample A0 shows only one band around 3300 cm^{-1} whereas sample A3 shows two bands at 3384 cm^{-1} and 3194 cm^{-1} characteristic of the hydroxyl stretching vibrations of water and goethite, respectively [18].

Raman spectroscopy and thermogravimetric analysis were performed on sample A3 in order to confirm that the as synthesized material consists of goethite. The Raman spectrum of sample A3 shows five shifts between 200 cm^{-1} and 600 cm^{-1} (Fig. 5) and their positions agree with those reported for α-FeOOH [19]. The TGA and DTG curves of sample A3 depicted on Fig. 6 shows two thermal phenomena between 25 °C and 500 °C. The first phenomenon which occurs before 100 °C with a mass loss of 2.8% corresponds to the elimination of adsorbed water. The second one with a DTG peak at 250 °C corresponds to the transformation of goethite into hematite [20]. Indeed, the mass loss obtained for this process is 11.5% and is very close to the theoretical value of 10% calculated according to Eq. (5).

$$2\alpha\text{-FeOOH} \rightarrow \alpha\text{-}Fe_2O_3 + H_2O \quad (5)$$

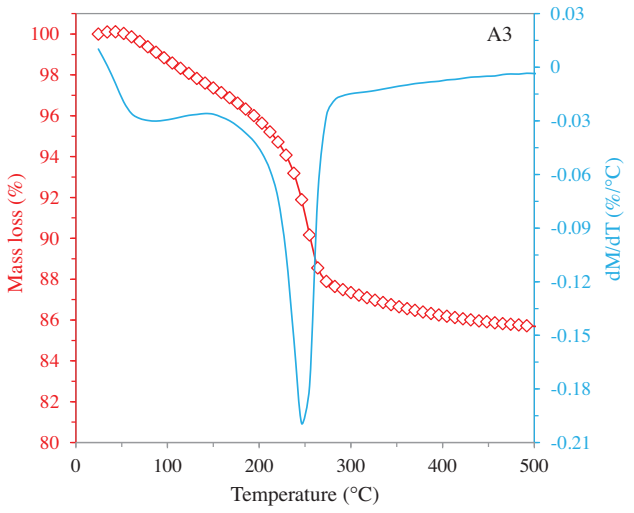

Fig. 6. TGA and DTG curves of the 3 h aged plasma-synthesized material (A3). The DTG peak at 250 °C corresponds to the dehydration of goethite into hematite.

Table 1
Textural properties of the plasma-synthesized materials.

Sample	S_{BET} ($m^2\ g^{-1}$)	Pore volume ($cm^3\ g^{-1}$)
A0	7	0.04
A1	69	0.12
A2	86	0.20
A3	134	0.30

Generally, the DTG peak representing the goethite-hematite transformation is sharp at 385 °C for highly crystalline goethite, but for the finely grained and poorly crystallized goethite, the dehydration temperature is always lower [21].

3.2. Textural properties of materials

Fig. 7 presents a series of SEM pictures of the plasma synthesized materials. The material recovered directly after the discharge was switched off (i.e. the non-aged A0 sample) shows numerous small particles with sizes of 200–500 nm (Fig. 7a). After ageing for 1 h, solid spheres (500 nm–1 μm in diameter) with small nanorods on their surfaces were obtained (Fig. 7b). As the ageing time was prolonged to 2 h, the spheres became larger (1–2 μm in diameter), and the nanorods on the surfaces grew longer and denser (Fig. 7c). After 3 h, uniform sea-urchin like hollow spheres were formed (Fig. 7d). This result shows that when the iron (II) solution is exposed to the plasma discharge, many iron (hydr) oxide nanoparticles are formed. During the ageing process, these nanoparticles spontaneously aggregated into large spheres to minimize the overall surface energy of the system. Subsequently, short nanorods were grown on the surfaces due to the preference of transition metal oxides for one-dimensional growth [22–24].

The nitrogen adsorption–desorption isotherms of the plasma-synthesized materials and their corresponding pores size distribution curves are presented on Fig. 8. The adsorption isotherm of all the samples is of type II (without occurrence of capillary condensation at intermediate partial pressures). They only differ by the amount of adsorbed N_2, which follow the respective specific surface areas of the samples (Table 1). The desorption isotherm of A0 perfectly follows the adsorption one. This combination of adsorption and desorption branches indicates that A0 is non-porous. On the contrary, for the samples A1–A3, a capillary decondensation is observed, revealing the presence of mesopores. The absence of capillary condensation at the adsorption and the occurrence of a capillary decondensation is characteristic of materials with slit-shaped mesopores. These may be related to the spaces between the nanorods of the sea-urchin like particles observed on SEM pictures as slits. The non-porous structure of sample A0 is confirmed by its pores size distribution curve which does not show any maximum corresponding to any specific pore size. For sample A1, the distribution curve presents a single maximum at 3.8 nm, indicating a good homogeneity in pores distribution for such material. For sample A2, the curve shows two maxima, indicating a bimodal pores distribution in the material. The first mode at 3.8 nm already observed on sample A1 corresponds to the pores in between the rods while the second one at 5.5 nm reveals the beginning of hollow spheres formation. The latter is confirmed by the pores size distribution curve of sample A3, which exhibits a single maximum at 5.4 nm. The surface area values of the synthesized materials and their pore volumes are summarized in Table 1. The surface area of the materials and their pore volume increased significantly with the ageing process. The surface area of the plasma-synthesized goethite obtained after ageing for 3 h (sample A3) is 134 $m^2\ g^{-1}$. This value is well above those generally obtained when goethite is synthesized without any surfactant [25]. The plasma technique

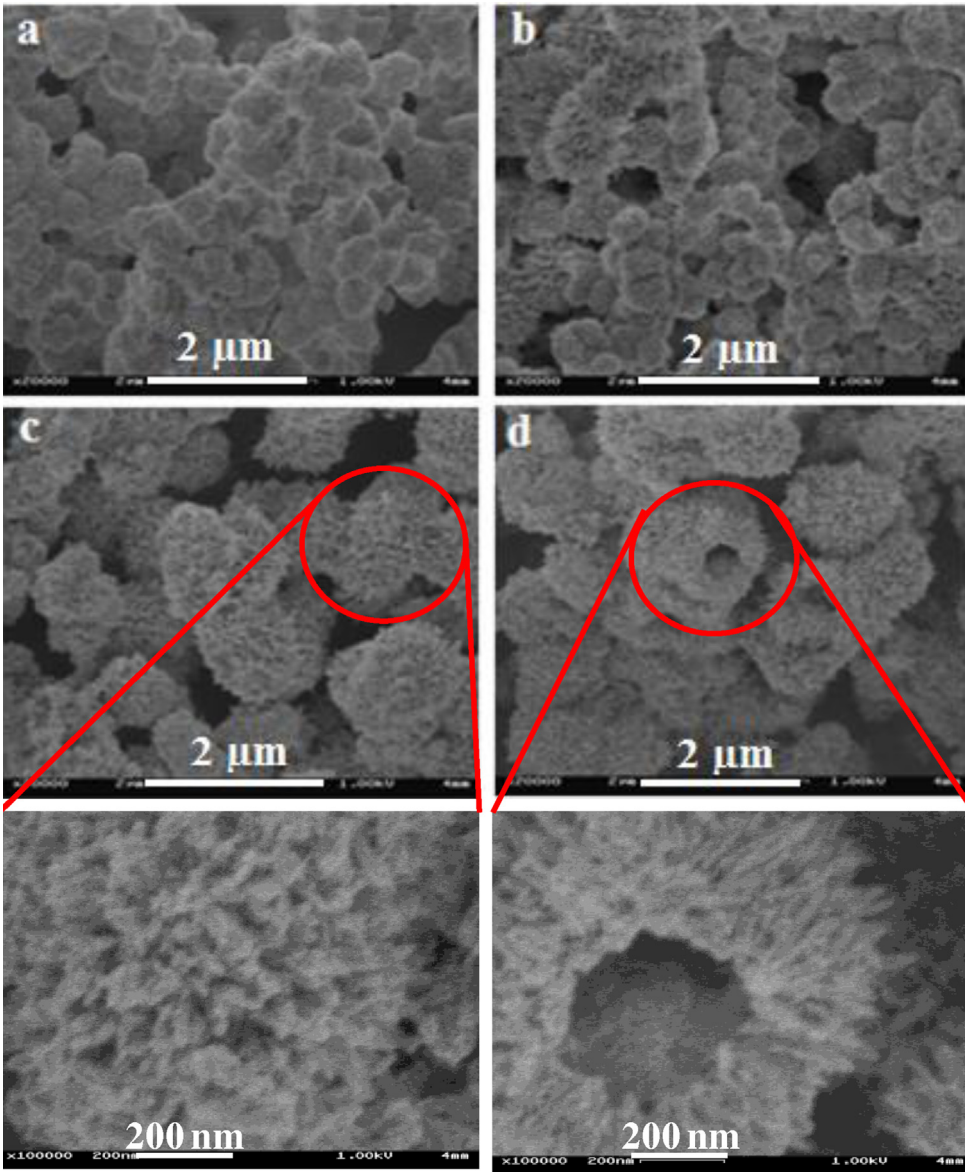

Fig. 7. SEM pictures of (a) non-aged material A0 and materials aged for (b) 1 h A1, (c) 2 h A2 and (d) 3 h A3; the zoom of pictures (c) and (d) clearly shows that the particles of plasma synthesized goethite look like sea-urchin hollow spheres.

used here can thus be presented as a "green" route for synthesis of mesoporous goethite with high surface area.

3.3. Mechanism of sea-urchin like goethite formation

Recently, Bratescu et al. have demonstrated that the synthesis of iron oxide/hydroxide nanoparticles by using pulsed liquid plasma is mainly the consequence of the redox properties of reactive species created in the plasma discharge [26]. The synthesis mechanism described by these authors showed that the hydroxyl radical produced by the discharge play a crucial role in such process. Since the hydroxyl radical created by humid air gliding arc plasma is one of the main impinging species that can react with aqueous species at the plasma-liquid interface (Fig. 9), Eqs. (6)–(8) were proposed to depict the mechanism of goethite synthesis from iron(II) solution. Because of the low pH value of the suspension (pH ≈ 2.2 after 60 min), the as produced hydroxyl radicals should be neutralized by H_3O^+ ions trough acid-base reaction. In spite of that, the iron precipitate was formed. This suggests that the precipitation reaction is probably more rapid than the acid-base one.

(i) Oxidation of ferrous ions into ferric ions by the hydroxyl radicals

$$Fe^{2+} + HO^{\bullet} \rightarrow Fe^{3+} + HO^{-} \quad (6)$$

(ii) Precipitation of ferric ions into iron oxyhydroxide

$$Fe^{3+} + 2HO^{-} + H_2O \rightarrow FeOOH + H_3O^{+} \quad (7)$$

(iii) Precipitation of non-oxidized ferrous ions into iron oxyhydroxide

$$2Fe^{2+} + 4HO^{-} \rightarrow 2FeOOH + H_2 \quad (8)$$

These equations clearly show that the process starts by a redox reaction (oxidation of ferrous ions into ferric ions). The hydroxyl ions produced by this redox reaction are then used as a precipitation reagent to form iron (hydr) oxide nanoparticles which then further transform into the α-FeOOH sea-urchin like hollow spheres after being aged for three hours (Fig. 9). Ageing the as synthesized iron (hydr) oxide was done only to allow structural rearrangements leading to the formation of porous and crystalline material. No analyses were done to follow the fate of the sulfate and ammonium ions

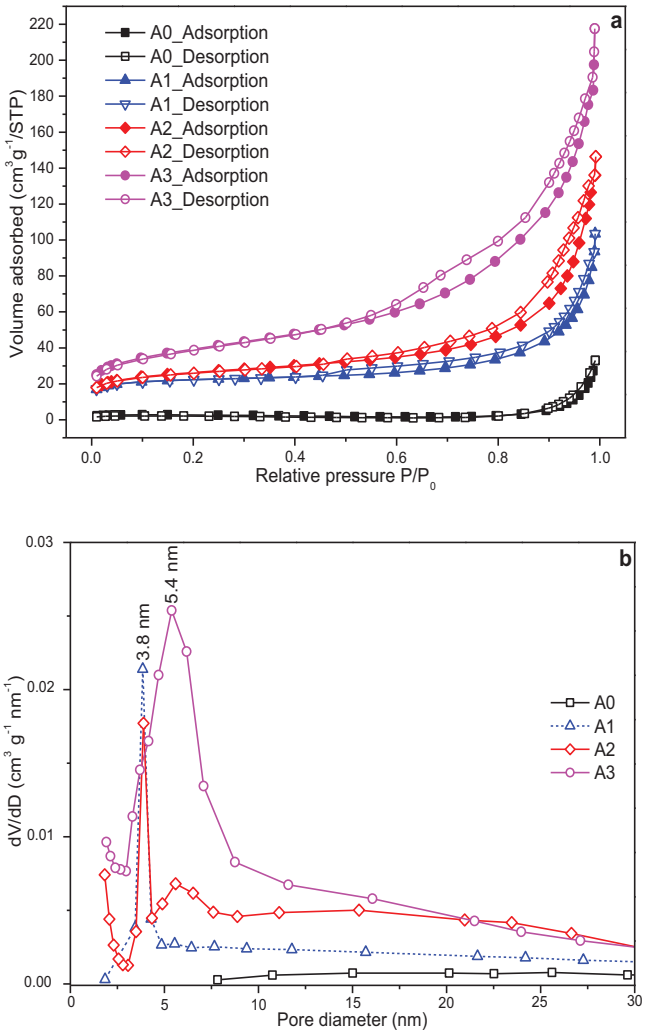

Fig. 8. N_2-physisorption isotherms (a) and pores size distribution as measured by the BJH method on the desorption isotherms (b) of the non-aged and aged materials.

after the plasmachemical oxidation–precipitation of iron(II) ions. However, it is possible that the ammonium ions were oxidized into NOx by the plasma species.

3.4. Catalytic degradation of Orange II

The bleaching of OII via a Fenton reaction catalysed by a plasma-synthesized goethite was followed qualitatively and quantitatively. Fig. 10a shows that the initial OII solution presents one absorption band ($\lambda = 485$ nm) in the visible region. This band corresponds to electronic transitions associated with the N=N chromophore groups responsible for the orange colour of the solution. This spectrum also has a band in the UV absorption region ($\lambda = 310$ nm) corresponding to electronic transitions related to the carbon–carbon double bonds of the aromatic rings present in the dye structure. During the catalytic treatment of the dye solution, there is a gradual and simultaneous decrease in the intensity of the two absorption bands. The decrease in intensity of the band at 485 nm is related to the bleaching process whereas that of the band at 310 nm is related to the oxidative degradation of benzene and naphthalene rings of the dye molecules. The heterogeneous Fenton degradation of OII can be described by Eqs. (9)–(12) as reported in many previous works [28,29]. The symbol (≡) represents the solid surface of goethite.

$$\equiv Fe^{3+} + H_2O_2 \rightarrow \equiv Fe(OOH)^{2+} + H^+ \quad (9)$$

$$\equiv Fe(OOH)^{2+} \rightarrow \equiv Fe^{2+} + HO_2^{\bullet} \quad (10)$$

$$\equiv Fe^{2+} + H_2O_2 + H^+ \rightarrow \equiv Fe^{3+} + H_2O + HO^{\bullet} \quad (11)$$

$$HO^{\bullet} + \text{OIImolecules} \rightarrow \text{Degradationproducts} \quad (12)$$

The quantitative analysis of OII bleaching kinetics was performed by measuring the absorbance of the solution at 485 nm (Fig. 10b). It is seen that the combination of H_2O_2 with plasma-synthesized goethite provides a greater dye bleaching. During the 10 first minutes, a fast bleaching is observed in the presence of the catalysts. This is then followed by a less rapid bleaching which remains linear until the end of the test. The event at the beginning of the test is likely due to the initial fast adsorption of OII at the surface of the solids, whereas the second part likely correspond to a catalytic modification of the pollutant. The maximum bleaching efficiency was 78% after 120 min. While replacing the plasma-synthesized goethite by a commercial goethite (Aldrich, $S_{BET} = 35\ m^2\ g^{-1}$), the obtained bleaching efficiency was 73%, suggesting that the activity of the plasma synthesized catalyst is comparable to that of commercial goethite. It is well known that the organic dye bleaching does not mean its total mineralization. The mineralization efficiency of OII dye by Fenton reaction in the presence of the synthesized goethite was evaluated by measuring the total organic carbon (TOC) of the solution. As shown in Fig. 11,

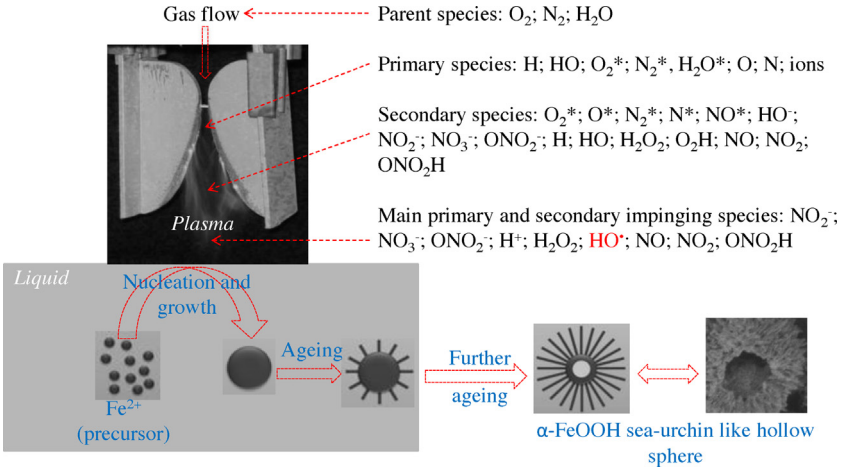

Fig. 9. Schematic view of the preparation of α-FeOOH sea-urchin like nanostructures by the gliding arc plasma process; the distribution of the reactive species is adapted from [16] and [27].

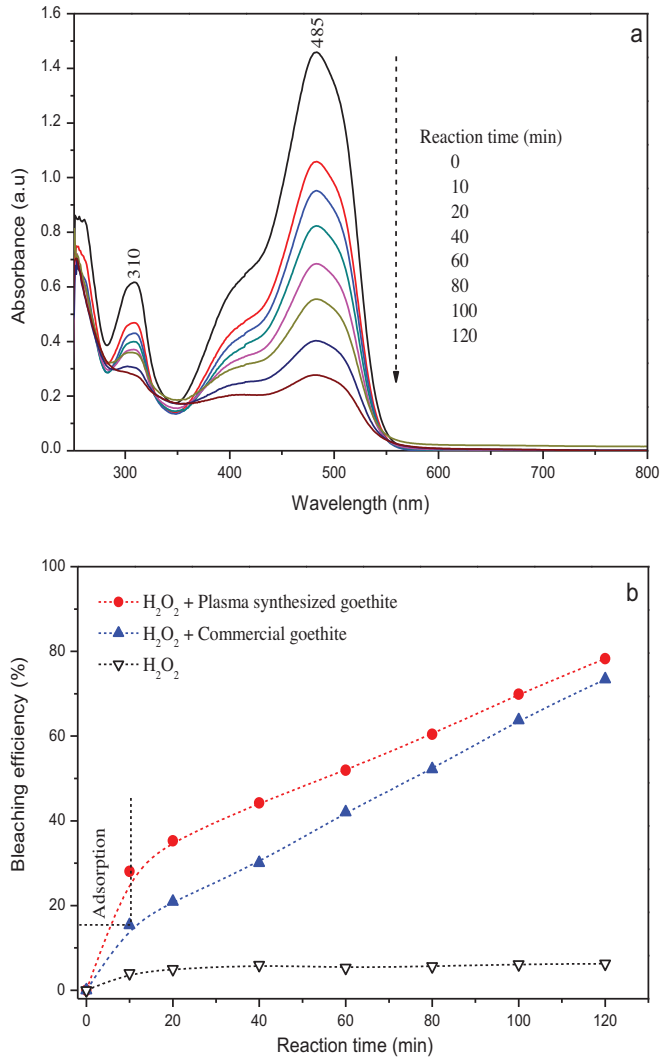

Fig. 10. Evolution of the UV–visible spectrum (a) and bleaching efficiency (b) of a 25 mg L^{-1} OII solution with reaction time (initial solution pH: 3, catalyst dosage: 0.2 g L^{-1}; H_2O_2 concentration: 5 mM; reaction temperature: 30 °C).

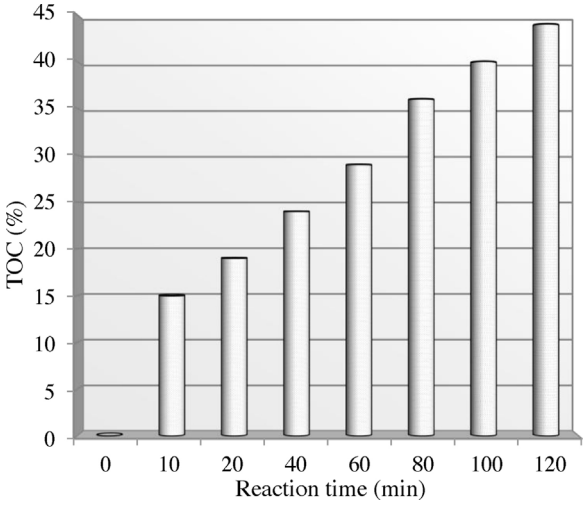

Fig. 11. Evolution of the mineralization efficiency as a function of reaction time (initial solution pH: 3, catalyst dosage: 0.2 g L^{-1}; H_2O_2 concentration: 5 mM; reaction temperature: 30 °C).

only 45% of TOC was removed at the end of the test. This suggests that a large quantity of the bleaching by-products is still organic and is present in the treated solution.

4. Conclusion

The aim of this work was (i) to synthesize porous iron oxyhydroxides by using a gliding arc plasma process and (ii) to evaluate the catalytic performance of the as synthesized material in the heterogeneous Fenton degradation of Orange II. Results showed that the exposure of iron(II) solution to the plasma discharge induces the formation of amorphous and non-porous iron(III) (hydr) oxide. Ageing of this amorphous material resulted in the formation of sea-urchin like goethite. During the ageing process, the as synthesized material became porous and its surface area increased. The BET surface area of the plasma synthesized goethite was 134 m^2g^{-1}; this value is well above those generally obtained when goethite is synthesized without any surfactant. The Orange II bleaching efficiency was 78% and 73% when plasma-goethite and commercial-goethite were respectively used as heterogeneous Fenton catalyst, suggesting that the catalytic activity of plasma-synthesized goethite is comparable to that of its commercial counterpart.

Acknowledgements

The authors thank the "Université catholique de Louvain" (Belgium) for the grant awarded to A. Tiya-Djowe in the frame of the fellowship "Coopération au développement" program. They are also grateful to Professor J.-L Brisset of "Université de Rouen" for the gliding arc plasma reactor support.

References

[1] C.Y. Cao, J. Qu, W.S. Yan, J.F. Zhu, Z.Y. Wu, W.G. Song, Langmuir 28 (2012) 4573–4579.
[2] F.Z. Mou, J.G. Guan, Z.D. Xiao, Z.G. Sun, W.D. Shi, X.A. Fan, J. Mater. Chem. 21 (2011) 5414–5421.
[3] S.W. Cao, Y.J. Zhu, J. Phys. Chem. C 112 (2008) 6253–6257.
[4] V. Tanboonchuy, J.C. Hsu, N. Grisdanurak, C.H. Liao, Environ. Sci. Pollut. Res. 18 (2011) 857–864.
[5] G. Zhang, S. Wang, F. Yang, J. Phys. Chem. C 116 (2012) 3623–3634.
[6] Y. Zhao, J. Hu, H. Chen, J. Photochem. Photobiol. A: Chem. 212 (2010) 94–100.
[7] L.S. Zhong, J.S. Hu, H.P. Liang, A.M. Cao, W.G. Song, L.J. Wan, Adv. Mater. 18 (2006) 2426–2431.
[8] S.Y. Zeng, K.B. Tang, T.W. Li, Z.H. Liang, D. Wang, Y.K. Wang, Y.X. Qi, W.W. Zhou, J. Phys. Chem. C 112 (2008) 4836–4843.
[9] M.C.S. Faria, R.S. Rosemberg, C.A. Bomfeti, D.S. Monteiro, F. Barbosa, L.C.A. Oliveira, M. Rodriguez, M.C. Pereira, J.L. Rodrigues, J. Hazard. Mater. 237 (2014) 47–54.
[10] F. Depenyou Jr., A. Doubla, S. Laminsi, D. Moussa, J.L. Brisset, J.-M. Le Breton, Corros. Sci. 50 (2008) 1422–1432.
[11] B. Benstaali, P. Boubert, B.G. Cheron, A. Addou, J.L. Brisset, Plasma Chem. Plasma Process. 22 (2002) 553–571.
[12] E. Acayanka, A. Tiya Djowe, S. Laminsi, C.C. Tchoumkwe, S. Nzali, A. Poupi Mbouopda, P.T. Ndifon, E.M. Gaigneaux, Plasma Chem. Plasma Process. 33 (2013) 725–735.
[13] A. Tiya Djowe, S. Laminsi, D. Njopwouo, E. Acayanka, E.M. Gaigneaux, Plasma Chem. Plasma Process. 33 (2013) 707–723.
[14] A. Tiya Djowe, S. Laminsi, E. Acayanka, R.G. Lontio Nkouongfo, E.M. Gaigneaux, J. Environ. Chem. Eng. (2014), http://dx.doi.org/10.1016/j.jece.2014.11.016.
[15] E. Njoyim-Tamungang, S. Laminsi, P. Ghogomu, D. Njopwouo, J.-L. Brisset, Chem. Eng. J. 173 (2011) 303–308.
[16] J.-L. Brisset, E. Hnatiuc, Plasma Chem. Plasma Process. 32 (2012) 655–674.
[17] H. Fan, B. Song, Q. Li, Mater. Chem. Phys. 98 (2006) 148–153.
[18] R.L. Frost, Z. Ding, H.D. Ruan, J. Therm. Anal. Calorim. 71 (2003) 783–797.
[19] D.L.A. de Faria, S. Venâncio Silva, M.T. de Oliveira, J. Raman Spectrosc. 28 (1997) 873–878.
[20] D. Walter, G. Buxbaum, W. Laqua, J. Therm. Anal. Calorim. 63 (2001) 733–748.
[21] Y.V. Swamy, B.B. Kar, J.K. Mohanty, Hydrometallurgy 69 (2003) 89–98.
[22] M. Hojamberdiev, G. Zhu, A. Eminov, K. Okada, J. Cluster Sci. 24 (2013) 97–106.
[23] J.M. Ma, A. Manthiram, RSC Adv. 2 (2012) 3187–3189.

[24] X.H. Xia, J.P. Tu, Y.Q. Zhang, Y.J. Mai, X.L. Wang, C.D. Gu, X.B. Zhao, RSC Adv. 2 (2012) 1835–1841.
[25] U. Schwertmann, R.M. Cornell, Iron Oxides in the Laboratory: Preparation and Characterization, 2nd ed., Wiley-VCH Verlag GmbH, D-69469 Weinheim (Federal Republic of Germany), 2000, pp. 180.
[26] M.A. Bratescu, N. Saito, O. Takai, Curr. Appl. Phys. 11 (2011) 30–334.
[27] S. Laminsi, E. Acayanka, S. Nzali, P.T. Ndifon, J.-L. Brisset, Deswater 37 (2012) 38–45.
[28] J. He, W. Ma, J. He, J. Zhao, J.C. Yu, Appl. Catal. B: Environ. 39 (2002) 211–220.
[29] I.S.X. Pinto, P.H.V.V. Pacheco, J.V. Coelho, E. Lorençon, J.D. Ardisson, J.D. Fabris, P.P. de Souza, K.W.H. Krambrock, L.C.A. Oliveira, M.C. Pereira, Appl. Catal. B: Environ. 119–120 (2012) 175–182.